

PCCP

Accepted Manuscript



This is an *Accepted Manuscript*, which has been through the Royal Society of Chemistry peer review process and has been accepted for publication.

Accepted Manuscripts are published online shortly after acceptance, before technical editing, formatting and proof reading. Using this free service, authors can make their results available to the community, in citable form, before we publish the edited article. We will replace this *Accepted Manuscript* with the edited and formatted *Advance Article* as soon as it is available.

You can find more information about *Accepted Manuscripts* in the [Information for Authors](#).

Please note that technical editing may introduce minor changes to the text and/or graphics, which may alter content. The journal's standard [Terms & Conditions](#) and the [Ethical guidelines](#) still apply. In no event shall the Royal Society of Chemistry be held responsible for any errors or omissions in this *Accepted Manuscript* or any consequences arising from the use of any information it contains.

Magnetic diffusion anomaly at the Néel temperature of pyrrhotite, $\text{Fe}_{1-x}\text{S}^\dagger$

F. William Herbert,^{a,b,c} Aravind Krishnamoorthy,^{a,b} Lucy Rands,^d Krystyn J. Van Vliet,^{a,c} and Bilge Yildiz^{*a,b}

Received Xth XXXXXXXXXXXX 20XX, Accepted Xth XXXXXXXXXXXX 20XX

First published on the web Xth XXXXXXXXXXXX 200X

DOI: 10.1039/b000000x

Cation diffusion is an important rate-limiting process in the growth of pyrrhotite (Fe_{1-x}S) in passivating films on steels exposed to sulfidic environments, and for proposed synthetic applications of Fe_{1-x}S , for example single-phase magnetic switching devices. Above the Néel temperature T_N of 315 °C, where Fe_{1-x}S is paramagnetic and structurally disordered, iron self-diffusivity $^*D_{\text{Fe}}$ predictably follows a standard, established Arrhenius law with temperature. However, we report ^{57}Fe tracer diffusion measurements below T_N , obtained using secondary ion mass spectrometry (SIMS), that demonstrate a 100-fold reduction in diffusion coefficient as compared to the extrapolated, paramagnetic Arrhenius trend at 150 °C. The results can be described by a magnetic diffusion anomaly, where the vacancy migration energy for the spontaneously-magnetized cation sublattice is increased by approximately 40% over the paramagnetic state. These constitute the first set of consistent diffusivity data obtained in magnetic pyrrhotite, allowing more accurate prediction of pyrrhotite growth rates and determination of magnetic properties for synthetic devices.

1 Introduction

Pyrrhotite (Fe_{1-x}S) barrier layers are important in passively protecting steels against highly sulfidizing and aggressive atmospheres, encountered in energy systems where hydrogen sulfide is present, such as oil and gas production and refining. One of the key protective qualities of pyrrhotite is to limit the rate of mass transport and hence general corrosion.^{1,2} Moreover, there has been recent interest in chemically fabricating low-dimensional, synthetic Fe_{1-x}S such as nanowires^{3,4} and nanodisks⁵ via solvothermal or electrodeposition methods. Such nanostructured Fe_{1-x}S crystals are promising for magnetic recording devices, in which the switching of magnetic states is controlled by cation-diffusion driven phase transformations.⁶ Ionic-diffusion-driven solid state reactions have also been used to create heteronanostructures of CuS_2 with Fe and Zn.⁷ In all of these cases, an accurate knowledge of Fe diffusivities in Fe_{1-x}S , as the key kinetic rate-limiting process in crystal growth or phase switch-

ing, is crucial to the design and prediction of the desired properties.

Fe_{1-x}S is an off-stoichiometric phase ($0 \leq x \leq 0.125$) which is paramagnetic and structurally disordered above its critical Néel temperature T_N of 315 °C.⁸ Below T_N , Fe_{1-x}S undergoes spontaneous magnetic ordering whereby co-planar Fe atoms normal to the crystal c -axis couple ferromagnetically and those in adjacent planes couple antiferromagnetically. Vacancy-vacancy interactions further lead to the formation of composition-dependent, ordered superstructures at low temperatures that govern overall, macroscopic magnetic properties.⁹ Previous measurements of Fe self-diffusion $^*D_{\text{Fe}}$ in paramagnetic Fe_{1-x}S have been carried out by several authors using thermogravimetric^{10–12} and radio-tracer^{13,14} methods, as compiled in Figure 1a. An isothermal spread in $^*D_{\text{Fe}}$ of approximately one order of magnitude is observed, stemming from variations in stoichiometry (Fig. 1a) or crystal anisotropy (Fig. 1b). Despite this, the results above ~ 320 °C follow a standard Arrhenius law as a function of temperature, given by $D = D_0 \exp[-Q_P/k_B T]$, where D_0 is a prefactor, Q_P is the activation energy for diffusion in the paramagnetic lattice, and k_B is Boltzmann's constant. Stoichiometry and anisotropy influence only D_0 .

However, Condit *et al.* predicted decades ago that vacancy ordering below T_N would lead to an increase in

† Electronic Supplementary Information (ESI) available: See DOI: 10.1039/b000000x/

^aDepartment of Materials Science and Engineering, Massachusetts Institute of Technology, Cambridge, MA, USA

^bLaboratory for Electrochemical Interfaces, Massachusetts Institute of Technology, Cambridge, MA, USA

^cLaboratory for Material Chemomechanics, Massachusetts Institute of Technology, Cambridge, MA, USA

^dDepartment of Materials Science, University of Oxford, Oxford, UK

the activation barrier for Fe self-diffusion.¹⁴ Indeed, the only available $^*D_{\text{Fe}}$ measurements at temperatures lower than ~ 300 °C, obtained via a unique magnetokinetic method (Figure 1a, data labelled "Z"), may substantiate this claim but for lack of auxiliary supporting data. In a separate study, we recently repeated these measurements and demonstrated them to be inaccurate.¹⁵ Nevertheless, the influence of the simultaneous magnetic/structural order-disorder transition at T_N on the diffusion coefficient of Fe in pyrrhotite remains an open question. An abrupt and discontinuous drop in D at a critical temperature is commonly observed in systems that undergo structural order-disorder transitions, due to a reduction in the concentration of mobile defects, for example in oxides such as Bi_2O_3 or $\text{La}_2\text{Mo}_2\text{O}_7$.¹⁶ On the other hand a more subtle, second-order change in the Arrhenius dependence of D , due to a change in the migration barrier energy, is seen in ferromagnets such as body-centered cubic iron, below their spontaneous magnetic ordering or Curie temperature T_C .¹⁷⁻¹⁹

Given the primary motivation to investigate the effect of the critical ordering temperature T_N on cation self-diffusion in pyrrhotite, we employed dynamic secondary ion mass spectrometry (SIMS) to measure diffusion profiles of the stable ^{57}Fe isotope tracer in Fe_{1-x}S . SIMS is a highly sensitive technique that permits depth profiling on the order of nanometers and hence allowed the use of very short annealing times and low temperatures in the range 170-400 °C. Our results above T_N are consistent with previous measurements obtained on disordered pyrrhotites with similar stoichiometry. In the ordered regime below ~ 315 °C, however, our $^*D_{\text{Fe}}$ results fall substantially below the extrapolated trend from the disordered pyrrhotite regime. Rather than vacancy ordering, we believe that the primary effect of spontaneous magnetic ordering at T_N causes this deviation in self-diffusivity. Based on a theoretical consideration of the influence of magnetic energy on vacancy formation and migration energies, we show that the activation energy Q_M for diffusion in fully, magnetically-ordered pyrrhotite is up to 41% higher than Q_P .

2 Methods

Sample preparation

Research-grade natural crystals of pyrrhotite were obtained from Ward's Science (Rochester, NY). Individual specimens had dimensions of approximately $5 \times 5 \times 5$ mm³ and were sourced from North Bend, WA. A representative sample of several individual crystals from the package was ground together into a powder in a

porcelain mortar for XRD phase identification (Figure 2a). Hexagonal pyrrhotite was found to be the only phase present (Inorganic Crystal Structure Database Ref. 00-050-1788). The position of the (10 $\bar{2}$) peak was used to estimate an average composition of 48.0 at% Fe, corresponding approximately to $\text{Fe}_{11}\text{S}_{12}$ (6C), or equivalently $x = 0.04$.²¹

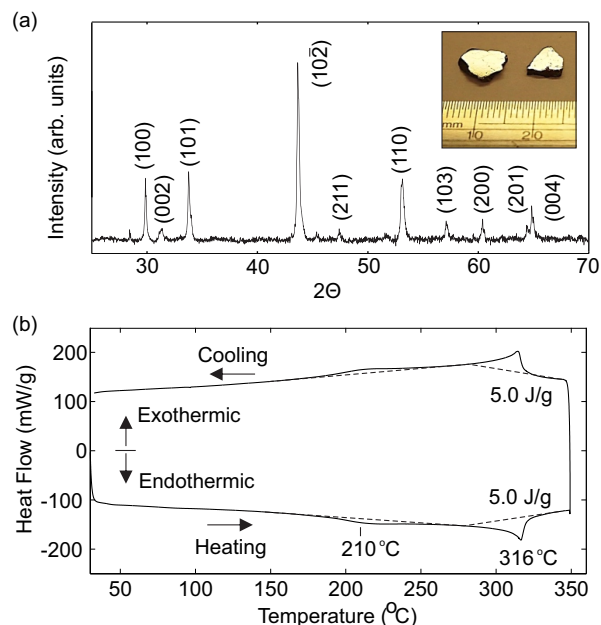


Fig. 2 (a) $\text{Cu-K}\alpha$ powder XRD pattern from a representative sample of research grade natural pyrrhotite; hexagonal Fe_{1-x}S peaks are labelled on the diagram. Inset: photographs of crystals; approximately $5 \times 5 \times 1$ mm³ polished to ≤ 50 nm roughness. The hexagonal Fe_{1-x}S (10 $\bar{2}$) peak's at 43.65° indicates an average composition of approximately 48.0 at% Fe. (b) Differential scanning calorimetry (DSC) loop from 30-300 °C, showing a heat uptake (release) upon heating (cooling) at 316 °C, corresponding to the critical order-disorder point of pyrrhotite.

The chemical composition of the natural crystals was investigated using energy-dispersive x-ray spectroscopy (EDS) in a JEOL 6610LV scanning electron microscope (SEM), to check for any large inclusions that may affect the reliability of the diffusion studies.[†] Potential metallic impurities such as Si and Al were not identified within the detection limit of the instrument (approx. 0.1 wt%)²², implying that any small inclusions were likely iron oxides. These were deemed sparse enough to not affect greatly the accuracy of the subsequent diffusion studies. The self-diffusion coefficient of iron in Fe_2O_3 is very small below 500 °C ($\leq 10^{-28}$ cm²s⁻¹)²³, so minor iron oxide inclusions were not expected to significantly influence Fe diffusion profiles. As-received crystals were polished down to 4000 grit sandpaper to achieve a flat surfaces

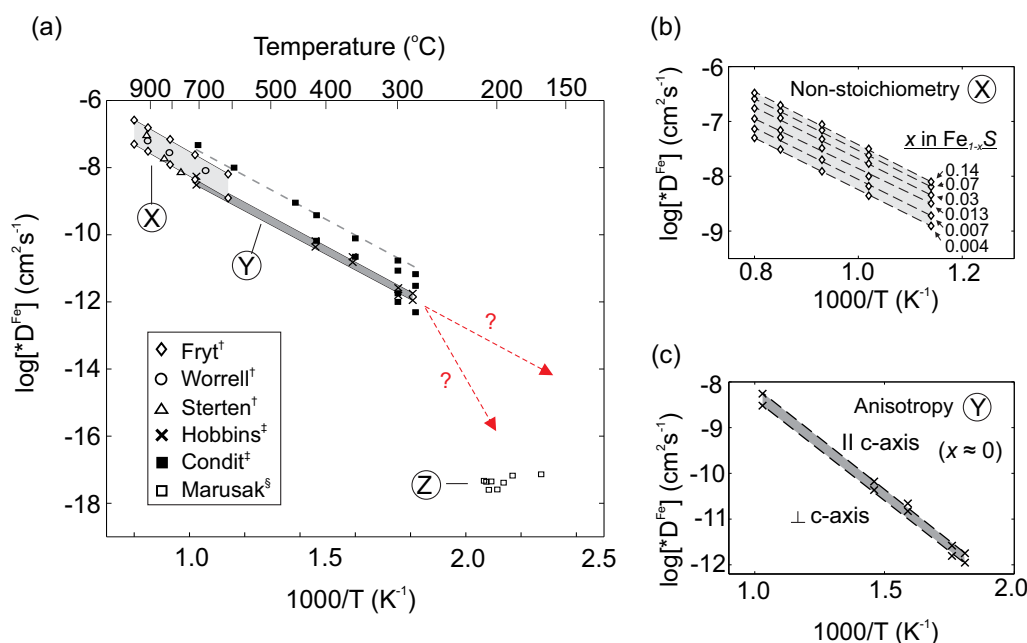


Fig. 1 Reported Fe self-diffusivity values. (a) Experimental $*D_{Fe}$ obtained using different techniques as listed. The aim of the current work was to measure a reliable set of data below 300°C. (b) Detail from region “X” on the main graph. Variations in stoichiometry x account for up to one order of magnitude variation in $*D_{Fe}$. (c) Detail from region “Y”: crystallographic anisotropy can account for half an order of magnitude variation. Data from: Fryt[†], Worrell[†], Sterten[†], Hobbins[‡], Condit[‡], Marusak[§]. († = sulfurization; ‡ = radiotracer; § = magnetokinetic measurements.)

followed by an extended polish of 5-10 min using 50 nm Al₂O₃ suspension. The resulting average surface root mean square (RMS) roughness, as measured by atomic force microscopy (AFM) was ≤ 50 nm.

Temperature-dependent magnetization studies confirmed that the natural pyrrhotite samples were antiferromagnetically ordered at room temperature. These samples also exhibited a peak-like, ferrimagnetic λ -transition starting at 160°C²⁰, followed by a full magnetic disordering to a paramagnetic state at ~ 315 °C.[†] Differential scanning calorimetry (DSC), shown in Figure 2b), demonstrated that a reversible, exothermic release of ~ 5 J/g at 316°C, which we attribute to a first-order, spontaneous disordering of vacancies upon loss of magnetic interactions at T_N .

⁵⁷Fe deposition and diffusion annealing

To study iron self-diffusion, the stable isotope ⁵⁷Fe was used as a tracer. ⁵⁷Fe has an abundance in natural iron of approximately 2%.²⁴ Solid chips of ⁵⁷Fe (96.06% enriched, Nakima Ltd., Israel) comprising a total mass of 200 mg were evaporated onto the surface of ~ 40 polished Fe_{1-x}S crystals simultaneously using a Sharon TE-1 thermal evaporator. The resulting deposit thickness,

measured *in situ* with a quartz crystal microbalance and confirmed *ex situ* by measuring a deposit shadow profile on a glass substrate, was 130 nm. Once coated in 130 nm of ⁵⁷Fe, pyrrhotite crystals were subjected to diffusion annealing runs at a range of temperatures between 170-400 °C for different lengths of time. Preliminary studies on synthetic thin film samples found that even small quantities of residual oxygen present during the annealing process had the effect of reducing the measured diffusivity by several orders of magnitude below expected values, due to the formation of an oxide film that tied up ⁵⁷Fe at the surface. Therefore, all bulk sample annealing was conducted in a horizontal quartz tube furnace under an O₂-free, dynamic H₂S:H₂ atmosphere in a molar ratio of 1:3500, which is within the sulfur partial pressure stability window for Fe_{1-x}S for the relevant range of temperatures.²⁵ Maintaining this reducing atmosphere prohibited the formation of oxide on the deposit or oxidation of the crystals themselves. Crystals were inserted into the hot section of the furnace for a predetermined duration before being removed outside the tube furnace for cooling under flowing H₂S/H₂. A thermocouple allowed *in situ* temperature profiles to be recorded for each annealing run.

Secondary Ion Mass Spectrometry (SIMS)

Depth profiling of annealed specimens was conducted in a CAMECA IMS-5f dynamic SIMS at the Materials Research Laboratory of the University of Illinois (Urbana-Champaign, IL). SIMS profiling to measure diffusivity has been shown to accurately replicate bulk self-diffusion results from traditional radiotracer measurement techniques for hematite, Fe_2O_3 single crystals.²³ ^{57}Fe and ^{56}Fe depth profiles were established by using a 10-keV O^- primary ion beam. In addition to these two species, the instrument was calibrated to detect any metallic impurity elements (mainly Si, Al, Ca, Mg) during each measurement. Only areas of the samples where the signal from these impurities was below the detection limit of 10 ppm were used for diffusion analysis. Anions such as sulfur and oxygen could not be simultaneously measured along with cations using the O^- primary beam, and we do not include an analysis of these species in this work. The ^{57}Fe concentration $[^{57}\text{Fe}]$ as a function of sputtering time was determined from the intensities I of the secondary positive ions $^{56}\text{Fe}^+$ and $^{57}\text{Fe}^+$ using:

$$[^{57}\text{Fe}] = \frac{I(^{57}\text{Fe})}{I(^{57}\text{Fe}) + I(^{56}\text{Fe})} \quad (1)$$

Conversion of sputtering time to profile depth was achieved by measuring the depth of the SIMS craters using a Dektak profilometer and assuming a constant sputtering rate.[†] Diffusion profiles were fit to appropriate error function solutions discussed below, using MATLAB R2012b.

3 Results and Discussion

Fitting of diffusion profiles

Figure 3 compares the $[^{57}\text{Fe}]$ diffusion profile of an unannealed sample with the original ^{57}Fe deposit versus a typical profile of an annealed sample (275°C, 5 minutes). The original SIMS spectra as a function of time for the annealed sample are inset in the figure. The unannealed profile contains a sharp interface between the original ^{57}Fe deposit and the Fe_{1-x}S crystal, located at 130 nm depth. After annealing, a $[^{57}\text{Fe}]$ tail from diffusion extends approximately 800 nm into the crystal. Nevertheless, even after diffusion annealing at 275 °C, a substantial proportion of the initial, pure ^{57}Fe remained on the Fe_{1-x}S surface. This essentially acted as a semi-infinite source of isotopic iron in the limit of the relatively short annealing times used in this work. We can therefore assume the concentration at the diffusion couple interface (i.e., at 130 nm depth) is fixed at $c = c_0$ for the duration of

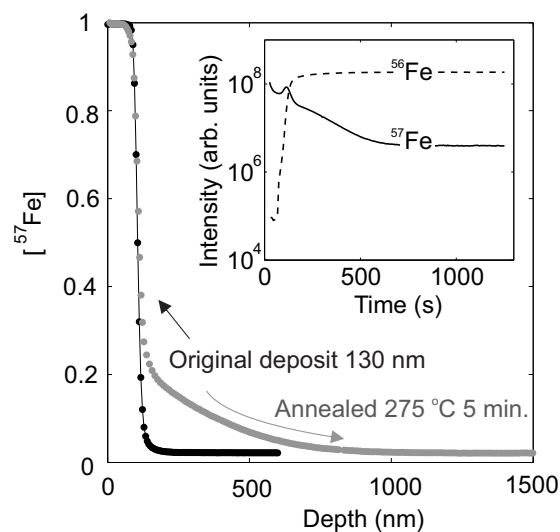


Fig. 3 The interdiffusion of a 130 nm-thick ^{57}Fe deposit on Fe_{1-x}S crystals was measured by secondary ion mass spectrometry (SIMS). The black curve shows the SIMS profile from an unannealed sample, indicating the depth of the original deposit. Inset: raw SIMS data for a sample annealed for 5 minutes at 275 °C; converted in the main plot to ^{57}Fe concentration vs. depth into the crystal (grey curve).

the annealing run. The initial and boundary conditions are hence:

$$c(x, t = 0) = 0 \quad (2)$$

and:

$$c(x = 0, t) = c_0 \quad (3)$$

Then it can be shown there exists an error function solution to Fick's second law in the form²⁶:

$$c(x, t) = c_0 \left[1 - \text{erf} \left(\frac{x}{4Dt} \right) \right] \quad (4)$$

The diffusion tails beyond the 130 nm original deposit were normalized to an initial, interfacial concentration $c_0 = 1$ and fit using Eq. (4). Figure 4 shows an example of fitting two profiles from samples annealed at the same temperature of 225°C but for different times of 1.8×10^3 and 1.3×10^4 s. The sample annealed longer exhibited a ^{57}Fe profile that extends further into the sample, as expected. However, the measured $^*D_{\text{Fe}}$ values from fitting were similar: 4.6 and 3.4×10^{-13} , respectively. Wherever possible, more than one measurement at a single temperature was obtained to check for consistency. The best-fit error function solutions are overlaid on top of experimental data with a range of uncertainty in Figure 4.[†]

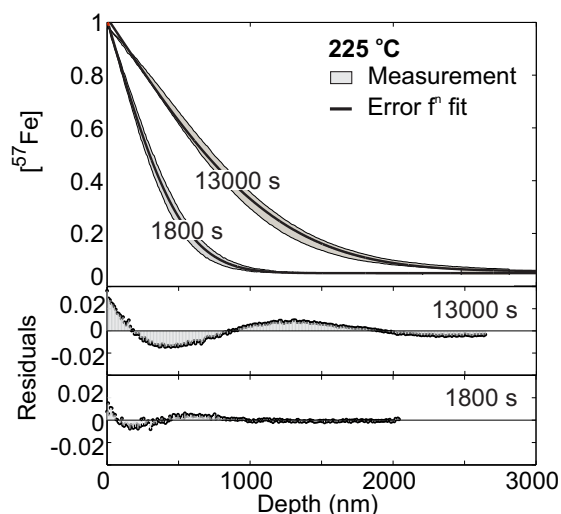


Fig. 4 The tail of each diffusion profile was fit with an error function solution (Eq. 4). Example fits for two samples annealed at 225 °C for approx. 1800 and 13000 s are shown.

3.1 Increased diffusion activation energy from spontaneous magnetization

Values of ${}^*D_{\text{Fe}}$ obtained from error function fitting are shown in Arrhenius form in Figure 5, alongside representative literature results from Fryt *et al.*¹⁰ and Condit *et al.*¹⁴, whose data are also displayed in Figure 1.[†] We include for comparison only those data corresponding to the stoichiometry range $0.03 \leq x \leq 0.1$ in Fe_{1-x}S , which is close to the composition of our samples analyzed via SIMS. Above ~ 315 °C, our measurements are consistent with the previous results, corresponding to an activation energy $Q_P = 0.83 \pm 0.03$ eV, representing the mean and standard deviation slopes obtained by regression fitting.

From Figure 5, we also observe that below T_N our ${}^*D_{\text{Fe}}$ values are considerably lower than the extrapolated Arrhenius trend with a slope of $-Q_P/k_B$. A deviation of this type beginning around 300 °C was previously observed by Condit *et al.*, who postulated that vacancy ordering reduced the number of mobile vacancies by fixing Fe vacancies in equilibrium superlattice positions, characterized by long residence times. Despite this observation, their experiments were not pursued to low enough temperatures to confirm this hypothesis or to quantify the activation energy in the new regime. In this study, we also considered the possibility that vacancy ordering may produce the observed, anomalous behavior at $T \leq T_N$. By comparison, however, oxides that undergo structural order-disorder transitions display large, discontinuous drops in diffusivity, by up to several orders of magnitude, at the critical ordering temperature.¹⁶ Conversely, the change

in Arrhenius behavior of ${}^*D_{\text{Fe}}$ in Figure 5 is continuous and does not seem to be consistent with the expected effect of a first-order structural reorganization. Rather, the transition is more reminiscent of the so-called “magnetic diffusion anomaly” observed at the paramagnetic-ferromagnetic critical point or Curie temperature T_C in ferromagnetic materials. Self-diffusion^{19,27,28} and solute diffusion^{18,29} in Fe, interdiffusion in Fe-Ni alloys³⁰ and, to a lesser extent, diffusion in Co¹⁹ all display a deviation from the Arrhenius law extrapolated from the paramagnetic region at T_C , characterized by a sharp spike or discontinuity in the effective activation energy Q_{eff} given by:

$$Q_{\text{eff}} = -k_B \frac{d(\ln D(T))}{d(1/T)} \quad (5)$$

In other words, the magnetic transition has a second-order effect on D , manifested in an abrupt change in Arrhenius slope. Ruch *et al.* derived a theoretical model for the magnetic diffusion anomaly, based on a constant diffusivity prefactor D_0 and a magnetic contribution to the activation energy for diffusion that varies with temperature as $S(T)^2$, where S is the reduced magnetization relative to magnetization at zero Kelvin: $S(T) = M(T)/M(T = 0\text{K})$.³¹ The generic diffusion coefficient in a magnetically ordered system can be written:

$$D(T) = D_0 \exp \left[-\frac{Q_P(1 + \alpha S(T)^2)}{k_B T} \right] \quad (6)$$

where the factor α includes the additive influence of magnetism on vacancy formation and migration energy terms. The ${}^*D_{\text{Fe}}$ data in Figure 5 are fit to Eq. (6) using the temperature variation of the (001)_{NiAs} magnetic reflection in synthetic Fe_7S_8 obtained by Powell *et al.*⁸ The factor α thus quantifies the magnetic ordering effect on the vacancy formation and migration energies, leading to an effective ferromagnetic activation energy for diffusion $Q_M = Q_P + \alpha S(T)^2$. From our results we obtained a best fit of $\alpha = 0.41 \pm 0.06$. In other words, the activation energy for diffusion at maximum magnetization (0 K) is approximately 1.18-1.30 eV, as opposed to 0.83 eV in the paramagnetic crystal at high temperatures. Additional fitting details are provided in the Supporting Information.[†] We assume here that the vacancy concentration remained fixed at the original bulk value of $C_V = 0.04$ during the annealing experiments. In other words, the effectively semi-infinite sample into which the Fe-57 exchanged remained at fixed stoichiometry. In this case, the increase in overall diffusion activation energy can be attributed solely to the magnetic influence on migration barrier.

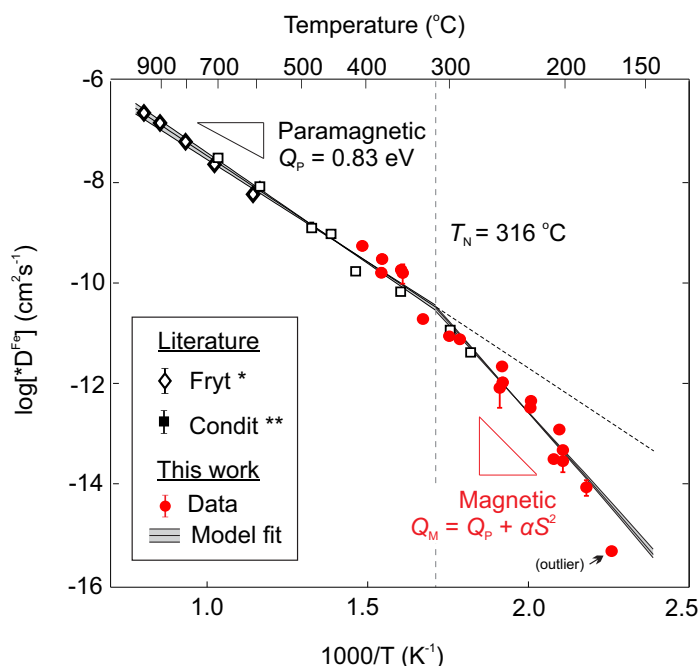


Fig. 5 Values for iron self-diffusion coefficient ${}^*D_{\text{Fe}}$ results obtained in this work are compared to data from Fryt *et al.*¹⁰ and Condit *et al.*¹⁴. The known magnetostructural ordering (Néel) temperature T_N of 316°C is indicated with a dashed line. Above T_N the activation energy slope in the paramagnetic state is $Q_p = 0.83 \pm 0.03$ eV. However, our results below T_N deviate below the extrapolated Arrhenius relationship. The data are fit using an activation energy Q_M for the spontaneously magnetized state that depends on reduced magnetization S as: $Q_M = Q_p + \alpha S^2$. The outlying data point at 170°C marked with an arrow is excluded from the trendline fit. Literature data correspond to pyrrhotite stoichiometries close to the samples used in this work (x in Fe_{1-x}S ~ 0.04): * Fryt, $x = 0.04$ ¹⁰; ** Condit, average of data from $0.03 \leq x \leq 0.1$.¹⁴

Nevertheless, it is worth adding a small comment regarding the reliability of our results as pure self-diffusivity measurements. Since Fe-57 was used as the tracer exchange material on top of the iron sulfide specimens, a small extent of chemical diffusion undoubtedly would have affected the measured diffusion profiles. The chemical contribution to diffusion arises from a small concentration gradient developing during annealing, altering the stoichiometry in the topmost, interdiffused volume towards a Fe:S ratio of 1:1. Such a chemical diffusion component would thus be expected to increase the diffusion rate and hence lead to a slight overestimate in self-diffusion values ${}^*D_{\text{Fe}}$. We did not quantify the extent of chemical diffusion contribution directly in our analysis, but, judging by the overlap of our data with the literature values in Figure 5, it is likely to be small. Moreover, any unintended but systematic overestimate in ${}^*D_{\text{Fe}}$ does not change the key observation of a magnetic diffusion anomaly, which leads to values considerably lower than the extrapolated, paramagnetic trend with temperature.

The implications of the magnetic diffusion anomaly in

pyrrhotite are twofold. First, the growth conditions for Fe_{1-x}S in solution both as a by-product of H_2S corrosion on iron and steels in energy infrastructure, as well as intentionally via solvothermal or electrodeposition methods for potential synthetic applications, are typically below 300°C. Therefore any *a priori* prediction of pyrrhotite growth rates from a consideration of cation diffusion must account for the effect of spontaneous magnetization, which reduces ${}^*D_{\text{Fe}}$ by up to 100-fold at 150°C when compared to a linear extrapolation of the Arrhenius slope from above the spontaneous ordering temperature. The accuracy of predictive tools for H_2S corrosion as well as more careful control of Fe_{1-x}S nanocrystal synthesis both stand to benefit from these findings. Second, although Fe_{1-x}S has long been studied for its interesting magnetic properties, to the authors' knowledge there is no example of a successful technological implementation of this material. Since the magnetic switching phenomena of interest in Fe_{1-x}S involve the local, diffusive rearrangement of vacancies, knowing the activation energy for Fe vacancy migration and formation in the magnetized state permits the development of simulation tools to design useful de-

vices from this material, such as temperature- and/or electric field-driven magnetic switching and memory applications.

4 Conclusions

In conclusion, ^{57}Fe tracer diffusion measurements were conducted to determine iron self-diffusivity $^*D_{\text{Fe}}$ in Fe_{1-x}S as a function of temperature in the range 170–400°C, which extends across the known magnetostructural order-disorder transition temperature $T_{\text{N}} = 315$ °C. Our results for $^*D_{\text{Fe}}$ above T_{N} agree well with measurements from previous studies in paramagnetic and structurally-disordered pyrrhotite, with an activation energy $Q_{\text{P}} = 0.83$ eV. However, below T_{N} , iron self-diffusivity deviates downwards from the extrapolated paramagnetic Arrhenius trend by approximately a factor of 10 at 200 °C and a factor of 100 at 150°C. This can be rationalized by considering a magnetic ordering effect on Fe vacancy migration energy, which increases the overall diffusion activation energy by up to 41% or to approximately 1.18–1.30 eV in the fully magnetically ordered state. To our knowledge, this work constitutes the first description of a magnetic diffusion anomaly in an ionic compound or a ferrimagnetic material. More practically, the knowledge of a magnetic contribution to diffusivity allows more accurate crystal growth rate and physical property predictions of ferrous sulfide barrier layers encountered in energy systems containing H_2S and other aggressive sulfidizing agents, as well as in the solution-based synthesis of Fe_{1-x}S at temperatures below 315°C.

5 Acknowledgements

We gratefully acknowledge the support provided by BP Plc. through the BP-MIT Center for Materials and Corrosion Research. We also appreciate the use of the CAMECA-5f Secondary Ion Mass Spectrometer at the Materials Research Center (MRC) of the University of Illinois, and in particular the assistance of Dr. Timothy Spila. FWH thanks Dr. Bal Mukund Dhar for extensive conversations and assistance in constructing equipment to make synthetic pyrrhotite films via Chemical Vapor Deposition for obtaining preliminary results.

References

- 1 H. Vedage, T. A. Ramanarayanan, J. D. Mumford and S. N. Smith, *Corrosion*, 1993, **49**, 114–121.
- 2 T. A. Ramanarayanan and S. N. Smith, *Corrosion*, 1990, **46**, 66–74.

- 3 G. H. Yue, P. X. Yan, X. Y. Fan, M. X. Wang, D. M. Qu, D. Yan and J. Z. Liu, *Journal of Applied Physics*, 2006, **100**, year.
- 4 M. Nath, A. Choudhury, A. Kundu and C. Rao, *Advanced Materials*, 2003, **15**, 2098–2101.
- 5 I. S. Lyubutin, C.-R. Lin, S.-Z. Lu, Y.-J. Siao, Y. V. Korzhetskiy, T. V. Dmitrieva, Y. L. Dubinskaya, V. S. Pokatilov and A. O. Kononova, *Journal of Nanoparticle Research*, 2011, **13**, 5507–5517.
- 6 T. Takayama and H. Takagi, *Applied Physics Letters*, 2006, **88**, year.
- 7 M. T. Mayer, Z. I. Simpson, S. Zhou and D. Wang, *Chemistry of Materials*, 2011, **23**, 5045–5051.
- 8 A. V. Powell, P. Vaquero, K. S. Knight, L. C. Chapon and R. D. Sánchez, *Physical Review B*, 2004, **70**, 014415.
- 9 H. Wang and I. Salveson, *Phase Transitions*, 2005, **78**, 547–567.
- 10 E. M. Fryt, W. W. Smeltzer and J. S. Kirkaldy, *Journal of The Electrochemical Society*, 1979, **126**, 673–683.
- 11 K. H. Worrell, W.L., in *Heterogeneous Kinetics at Elevated Temperatures*, Plenum Press, New York, 1970.
- 12 A. Sterten, *Corrosion Science*, 1974, **14**, 377–390.
- 13 R. Hobbins, *PhD thesis*, University of Delaware, 1970.
- 14 R. Condit, R. Hobbins and C. Birchenall, 1974, **8**, 409–455–.
- 15 F. Herbert, K. A., K. Van Vliet and B. Yildiz, *In preparation*, 2014.
- 16 A. J. Jacobson, *Chem. Mater.*, 2009, **22**, 660–674.
- 17 Y. Iijima, K. Kimura and K. Hirano, *Acta Metallurgica*, 1988, **36**, 2811–2820.
- 18 H. Nitta and Y. Iijima, *Philosophical Magazine Letters*, 2005, **85**, 543–548.
- 19 H. Ding, V. I. Razumovskiy and M. Asta, *Acta Materialia*, 2014, **70**, 130–136.
- 20 L. A. Marusak and L. N. Mulay, *Physical Review B*, 1980, **21**, 238–244.
- 21 R. G. Arnold, *Economic Geology*, 1969, **64**, 405–419.
- 22 R. Egerton, *Electron-energy loss spectroscopy in the electron microscope, 3rd Ed.*, Springer, 2011.
- 23 A. C. S. Sabioni, A. M. Huntz, A. M. J. M. Daniel and W. A. A. Macedo, *Philosophical Magazine*, 2005, **85**, 3643–3658.
- 24 <http://www.nndc.bnl.gov/chart/>.
- 25 P. Walder and A. Pelton, *Journal of Phase Equilibria and Diffusion*, 2005, **26**, 23–38.
- 26 R. Balluffi, S. Allen and W. Carter, *Kinetics of Materials*, Wiley, 2005.
- 27 B. Zhang, *AIP Advances*, 2014, **4**, year.
- 28 R. Perez and M. Weissmann, *Journal of Physics: Condensed Matter*, 2004, **16**, 7033.
- 29 R. Perez, D. Torres and F. Dymont, *Applied Physics A*, 2009, **97**, 381–385.
- 30 J. Yang and J. Goldstein, 2004, **35**, 1681–1690.
- 31 L. Ruch, D. R. Sain, H. L. Yeh and L. Girifalco, *Journal of Physics and Chemistry of Solids*, 1976, **37**, 649–653.